# Structural Origins of the Excellent Glass Forming Ability of $Pd_{40}Ni_{40}P_{20}$

P. F. Guan,[1] T. Fujita,[1] A. Hirata,[1] Y. H. Liu,[1] and M. W. Chen[1,2,*]

[1]*WPI Advanced Institute for Materials Research, Tohoku University, Sendai 980-8577, Japan*

[2]*State Key Laboratory of Metal Matrix Composites, School of Materials Science and Engineering, Shanghai Jiao Tong University, Shanghai 200030, People's Republic of China*

(Received 26 May 2011; revised manuscript received 22 September 2011; published 24 April 2012)

We report a hybrid atomic packing scheme comprised of a covalent-bond-mediated ''stereochemical'' structure and a densely packed icosahedron in a bulk metallic glass $Pd_{40}Ni_{40}P_{20}$. The coexistence of two atomic packing models can simultaneously satisfy the criteria for both the charge saturation of the metalloid element and the densest atomic packing of the metallic elements. The hybrid packing scheme uncovers the structural origins of the excellent glass forming ability of $Pd_{40}Ni_{40}P_{20}$ and has important implications in understanding the bulk metallic glass formation of metal-metalloid alloys.

DOI: 10.1103/PhysRevLett.108.175501 PACS numbers: 61.43.Bn, 61.05.cj, 61.43.Fs

The formation mechanisms of bulk metallic glasses (BMGs) with a very low critical cooling rate have been the recent topic of intense discussion [1–9]. In general, BMGs can be sorted into two groups: metal-metal–based glasses in which all components are metallic elements and metal-metalloid–based glasses that contain a large amount of metalloid elements, such as P, B, Si, and C. The excellent glass forming ability (GFA) of metal-metal–based BMGs has been attributed to the icosahedronlike local order because of the dense atomic packing along with lack of the translation symmetry for long-range growth [5–9]. However, for metal-metalloid–based BMGs, the discussion on local atomic structure is mixed and even controversial. Both covalent-bond-mediated ''stereochemical'' structure and random dense atomic packing have been reported [10–14]. Since the random dense packing is determined by the effective atomic size ratios [15], whereas the stereochemical packing is controlled by the saturation of directional covalent bonds [14], any specific requirements on bonding direction, coordination number, and coordinating atoms will affect the atomic packing density in a random manner. In principle, the two packing schemes cannot coexist in one uniform system. Therefore, it remains a mystery on the atomic structure of metal-metalloid BMGs as well as the underlying mechanisms of their GFA. In this Letter, we investigated the atomic structure of $Pd_{40}Ni_{40}P_{20}$, one of the best glass formers known since the 1980s [16], and uncovered a novel hybrid atomic packing scheme in metal-metalloid BMGs.

The *ab initio* molecular dynamics simulation with a canonical *NVT* (constant atom number, volume, and temperature) ensemble was accomplished by the Vienna *ab initio* simulation package [17]. The temperature was controlled by Nose-Hoover thermostat [18]. A projected augmented wave method [19] and generalized gradient approximation [20] were used to describe electron-ion interactions. The cooling process was performed on the Gamma point only, and the electronic properties were calculated based on dense $k$-point mesh. Cubic supercells with 200 atoms were initially constructed with a periodic boundary condition for $Pd_xNi_{80-x}P_{20}$ ($x = 0, 20, 40, 60$) alloys. The ensembles experienced a stepwise quenching process for glass structures. The details of the calculation can be found in the Supplemental Material [21]. The atomic structure of the alloys was also experimentally investigated by extended x-ray absorption fine structure (EXAFS) spectroscopy and high-energy x-ray diffraction (XRD) at the SPring-8 synchrotron radiation facility. The reliability of the simulated structures was statistically verified by the XRD and EXAFS spectra [see Supplemental Figs. S1(b)–(f)] [6].

The evolution of the generalized pair correlation function (PCF) of $Pd_{40}Ni_{40}P_{20}$ is shown in Fig. 1(a). The PCF exhibits a typical liquid behavior with a homogeneous atomic distribution at temperatures above 1200 K. The intensities of two characteristic peaks at ~2.5 and ~4.7 Å gradually increase, with temperatures decreasing. When temperatures are below 700 K, a shoulder peak in the front of the 2.5 Å peak emerges, and the 4.7 Å peak splits. The noticeable structure changes between 500 and 700 K are consistent with the known glass transition of $Pd_{40}Ni_{40}P_{20}$ at ~573 K [22]. The low-temperature (300 K) structure was further characterized by general [$g(r)$] and partial [$g_{ij}(r)$] radial distribution functions (RDF), as illustrated in Figs. 1(b) and 1(c). The calculated general RDF $g(r)$ has a good agreement with the experiment [10], further demonstrating the reliability of the simulated atomic configurations. Since the shoulder of the first peak in the PCF [Fig. 1(a)] approximately matches with the Ni-P and Pd-P bonding lengths [Fig. 1(c)], P-related short-range ordering appears to become remarkable during glass transition. The splitting of the P-Ni and P-Pd second peaks [Fig. 1(c)] is also in good agreement with the temperature-dependent peak separation in the PCF [Fig. 1(a)]. Moreover, the absence of a short $g_{PP}(r)$ peak in the RDF suggests that direct P-P bonds are rare in the alloy.

 

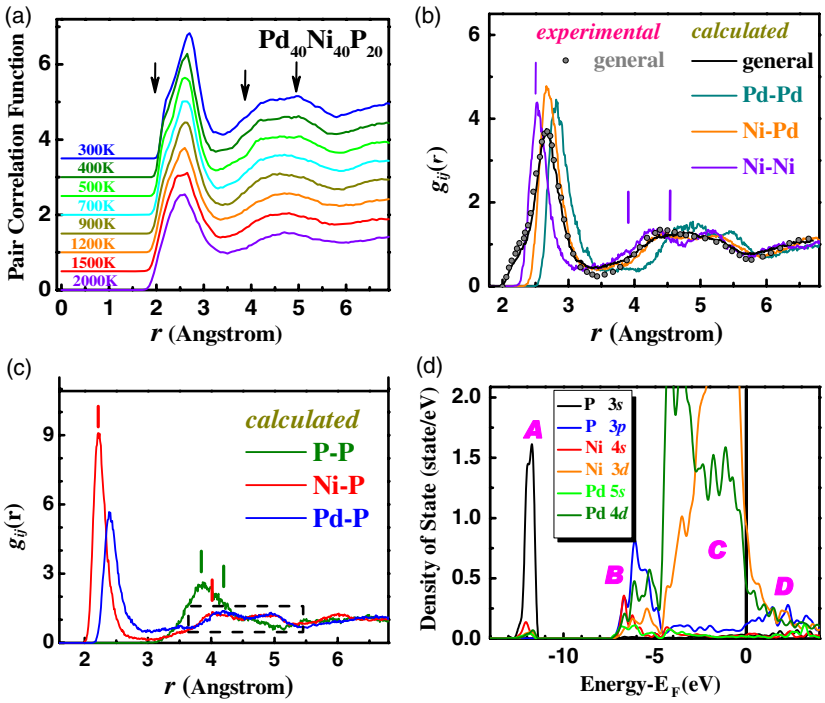


FIG. 1 (color online). (a) Simulated temperature-dependent pair correlation function of $Pd_{40}Ni_{40}P_{20}$ from 2000 to 300 K. The shoulder peak and subpeaks are marked by the arrowheads. (b),(c) The generalized and partial radial distribution functions of $Pd_{40}Ni_{40}P_{20}$. The experimental data are shown as a dotted line, and the calculated peaks of the hybrid packing assemblies are marked by solid lines. (d) The pDOS of $Pd_{40}Ni_{40}P_{20}$ for P, Ni, and Pd. **A**, **B**, **C**, and **D** are marked as the different bands for the discussion in the main text.

The partial density of states (pDOS) of $Pd_{40}Ni_{40}P_{20}$ is shown in Fig. 1(d). The pDOS can be divided into four bands: $-13\ \text{eV} < E\text{-}E_F < -11\ \text{eV}$ (marked as **A**), $-8\ \text{eV} < E\text{-}E_F < -5\ \text{eV}$ (**B**), $-5\ \text{eV} < E\text{-}E_F < 0\ \text{eV}$ (**C**), and $E\text{-}E_F > 0\ \text{eV}$ (**D**). **A** and **B** bands are contributed by the hybridization between the $3s$ and $3p$ electrons of P atoms and the $s$ and $d$ electrons of Ni and Pd atoms. The **C** band is mainly constructed by $3d$ electrons of Ni and Pd. There is an obvious "pseudogap" between **B** and **C** subbands in the profile of the $d$ band of Ni and Pd, indicating that a part of the $d$ electrons of Ni and Pd become localized due to hybridization. Moreover, the hybrid $p$-$d$ antibonding bands above the Fermi energy, $E_F$, can be observed in the band **D** [More evidence on the antibonding bands can be found in Fig. S3(b).] The presence of bonding and antibonding as well as the "localization" suggest the covalent-dominant bonding of P with Ni and Pd. Based on the pseudogaps that result from the electronic localization between P and Ni/Pd in $Pd_xNi_{80-x}P_{20}$ ($x = 20, 40, 60, 80$) glasses, we calculated the average electronic environment around P atoms (Fig. S2). The average electron number, belonging to the **A** and **B** bands for each P atom, is approximately 8 for the four glassy alloys, which is evidently associated with the saturation of covalent bonds of the four valence orbitals of P. In order to quantitatively describe the bonding nature, we plotted the spatial distributions of charge density within selected energy windows. The charge distribution of the band **C** shows that electrons are localized to individual atoms and do not have any contribution to the covalent bonding between P and Pd/Ni. Derived from the charge density distribution of the hybridized bands **A** and **B** ($-13\ \text{eV} < E\text{-}E_F < -5\ \text{eV}$), we plotted the three-dimensional isosurface with the charge density of $0.15\ \text{e}/\text{Å}^3$ [Fig. 2(b)]. The tube structure between P and Ni/Pd represents the covalence-like bonds as well as the charge redistribution duo to the orbital hybridization. Additionally, the partial covalent bonding between P and Ni/Pd is also revealed by the electron localization function and the different charge density distribution. The maximum value of the electron localization function between Ni and P in $Pd_{40}Ni_{40}P_{20}$ is as large as 0.80, demonstrating the covalence-dominated bonding behavior. The different charge density distribution further verifies the localization of electronic density between P and Ni/Pd (Fig. S3), whereas such behavior cannot be seen in Ni-Ni, Ni-Pd, and Pd-Pd atomic pairs.

We investigated the local atomic packing of the simulated glasses using the Voronoi tessellation method [23]. Since there is coexistence of covalent bonding between P and Ni/Pd and metallic bonding between Pd-Pd, Pd-Ni, and Ni-Ni in the glasses, it is more precise to define the cutoff values based on true interatomic bonding rather than average interatomic distances. In this Letter, the charge density at the middle points ($\rho_m$) of P-Ni and P-Pd bonds is used as the cutoff parameter for the P-centered polyhedra. The values are 0.21, 0.18, 0.15, 0.12 $\text{e}/\text{Å}^3$ for $Pd_xNi_{80-x}P_{20}$

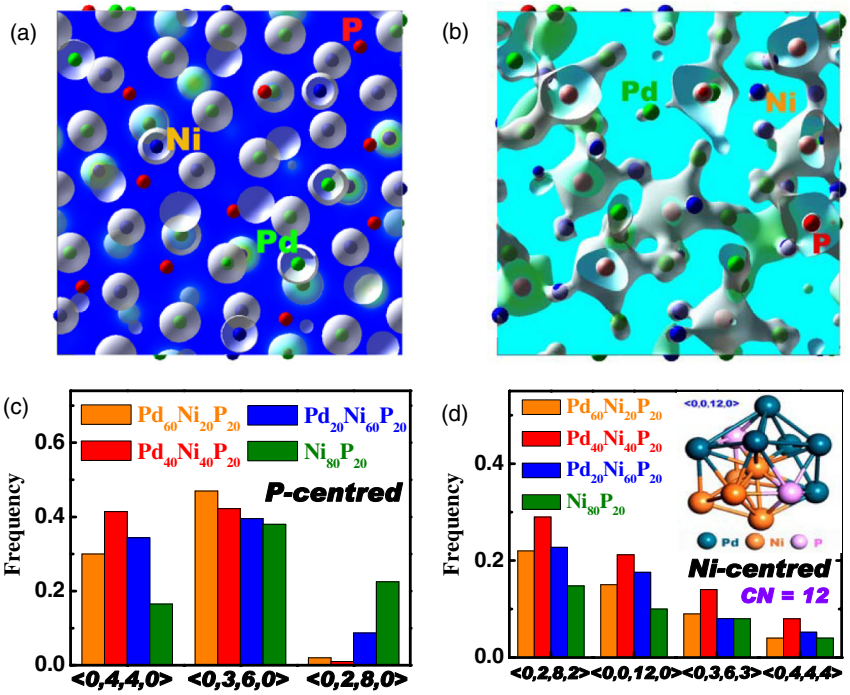


FIG. 2 (color online). (a) The isosurface of charge density of the band **C**, as shown in Fig. 1(d). (b) The isosurface of charge density of the bands **A** and **B** in Fig. 1(d). (c) The histogram of P-centered Voronoi polyhedra of $Pd_xNi_{80-x}P_{20}$ ($x = 0, 20, 40, 60$) glasses using charge density $\rho_m = 0.21, 0.18, 0.15, 0.12$ e/Å$^3$ as the cutoff parameters, respectively. (d) Histogram of Ni-centered Voronoi polyhedra for $Pd_xNi_{80-x}P_{20}$ ($x = 0, 20, 40, 80$) glasses. The frequencies are normalized by the atomic number of P. $R_{\text{cutoff}} =$ 3.5 Angstrom.

($x = 0, 20, 40, 60$), respectively (see Fig. S4). The distribution of the P-centered polyhedra is shown in Fig. 2(c), which is quite different from that based on interatomic distances (Fig. S4). In Fig. 2(c), three types of P-centered polyhedra with indices of $\langle 0, 3, 6, 0\rangle$ [tricapped trigonal prism (TTP)], $\langle 0, 4, 4, 0\rangle$ (distorted TTP), and $\langle 0, 2, 8, 0\rangle$ are frequently observed. Their distributions are correlated with the Pd/Ni concentration ratios in $Pd_xNi_{80-x}P_{20}$. For the binary $Ni_{80}P_{20}$ ($x = 0$), the P-centered $\langle 0, 3, 6, 0\rangle$ TTP is the foremost structure unit, which is well consistent with previous reports [14]. However, for the ternary alloys, both $\langle 0, 3, 6, 0\rangle$ TTP and $\langle 0, 4, 4, 0\rangle$ distorted TTP are the dominant polyhedra and the frequencies of $\langle 0, 3, 6, 0\rangle$ and $\langle 0, 4, 4, 0\rangle$ are almost identical in $Pd_{40}Ni_{40}P_{20}$.

Since there is significant metallic bonding [the band **C** in Fig. 1(d)] in the ternary glassy alloys, the atomic packing amongst metal atoms appears to be important for the overall atomic arrangements. We thus investigated Ni- and Pd-centered Voronoi polyhedra. There are no frequency favorable Pd-centered polyhedra [Fig. S5 (a)], whereas Ni-centered polyhedra with Voronoi indices of $\langle 0, 0, 12, 0\rangle$ and $\langle 0, 2, 8, 2\rangle$ show high frequencies in $Pd_xNi_{80-x}P_{20}$ [Fig. 2(d)] [24]. Interestingly, $Pd_{40}Ni_{40}P_{20}$ possesses the highest frequencies of $\langle 0, 0, 12, 0\rangle$ and $\langle 0, 2, 8, 2\rangle$ polyhedra that correspond to the dense atomic packing with icosahedronlike structures ($CN = 12$) [see the inset of Fig. 2(d)].

As the formation of the icosahedronlike polyhedra is driven by dense atomic packing with the maximal overlapping of valence electron density, the dominant bonding prefers to be directionless metallic bonds. In principle, the directional covalent bonds are not favorable for the densely packed icosohedra, since any specific requirements on bonding direction, coordination number, and coordinating atoms will naturally limit the atomic packing density in a random manner. We thus investigated the correlation between P-centered TTPs and Ni-centered icosahedra in

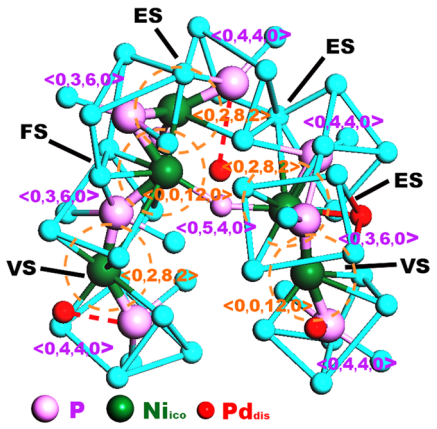


FIG. 3 (color online). Typical atomic configuration of glassy $Pd_{40}Ni_{40}P_{20}$. The connection between P-centered TTPs and Ni-centered icosahedra is highlighted, illustrating a topological order between the two clusters. FS, ES, and VS denote the face, edge, and vertex sharing methods between P-centered clusters. The dashed circles delineate the Ni-centered icosahedronlike polyhedra.

$Pd_{40}Ni_{40}P_{20}$. As shown in Fig. 3, there is a topological order between the two clusters. In general, one Ni atom, as a center of an icosahedronlike polyhedron, links two (sometimes three) P atoms that act as the centers of neighboring TTP clusters, while the Ni-centered icosahedron shares all the constituent atoms with the neighboring TTP clusters. It is worth noting that these Ni-centered polyhedra are usually accompanied by a P-centered $\langle 0, 4, 4, 0\rangle$ cluster, which is in accordance with the result that the fractions of both Ni-centered icosahedra and P-centered $\langle 0, 4, 4, 0\rangle$ clusters increase concurrently with the improved GFA of $Pd_xNi_{80-x}P_{20}$ [Figs. 2(c) and 2(d)]. Based on the hybrid packing scheme, we estimated the theoretical composition of the best glass former in this alloy system. The average composition of Ni-centered icosahedra is $Pd_{5.7}Ni_{3.9}P_{2.4}$, and the corresponding effective atomic size ratio is ~0.93, which is close to the ideal value of 0.902 for the random dense packing. This further confirms that the arrangement of metallic elements in the metal-metalloid glass follows the random dense packing scheme. The average composition of the P-centered TTPs (considering both $\langle 0, 3, 6, 0\rangle$ and $\langle 0, 4, 4, 0\rangle$) is $Pd_{4.0}Ni_{4.7}P_1$, which basically satisfies the rule of the charge saturation of P. Apparently, the composition of the best glass former is not just dependent on either the Ni-centered icosahedra or P-centered TTPs. The ideal composition should be the average composition of the hybrid clusters, comprised of Ni-centered icosahedrons and a P-centered TTP or distorted TTP, to satisfy both the dense packing of the metallic atoms and charge saturation of the metalloid components. The average composition of the hybrid clusters is estimated to be $Pd_{44.1}Ni_{38.3}P_{17.6}$, very close to the optimal composition, $Pd_{40}Ni_{40}P_{20}$, determined by the experiment.

To understand the intrinsic correlation between Ni-centered icosahedra and P-centered TTPs, we studied the atomic structures of P-centered $\langle 0, 4, 4, 0\rangle$ and $\langle 0, 3, 6, 0\rangle$ polyhedra [Fig. 4(a)]. The $\langle 0, 3, 6, 0\rangle$ polyhedron has a typical TTP structure, with six atoms at the vertices of the trigonal prism (denoted as site 1) and three atoms at sides of the prism (denoted as site 2). Although the $\langle 0, 4, 4, 0\rangle$ cluster can be considered as the tetragonal dodecahedron, it is actually the $\langle 0, 3, 6, 0\rangle$ TTP with a missing atom at site 2. According to the recent calculation [11], the absence of one metal atom at site 2 has an insignificant influence in the structural stabilization of TTP. This is probably because the covalent bonding saturation of a P atom only needs 8 electrons from the nearest Ni and Pd atoms. The typical atomic packing of P-centered TTPs with a Ni-centered polyhedron is illustrated in Fig. 4(b), in which the P-centered $\langle 0, 3, 6, 0\rangle$ and $\langle 0, 4, 4, 0\rangle$ clusters are linked together by a Ni-centered $\langle 0, 2, 8, 2\rangle$ polyhedron. It is interesting to note that the $\langle 0, 4, 4, 0\rangle$ cluster can be reverted to the $\langle 0, 3, 6, 0\rangle$ TTP by simply shifting the marked atom (red ball) from site **B** to site **A**. However, this operation breaks the icosahedral symmetry of the Ni-centered polyhedron [see the inset of Fig. 4(b) and Fig. S6]. Thus, there is an energy competition between the destruction of P-centered TTPs and Ni-centered icosahedra. We calculated the total energies of two atomic configurations with the atom at sites **A** and **B** (Fig. S6), respectively, and found that site **B** is more energy favorable with ~0.10 eV/atom lower than site **A** [25].

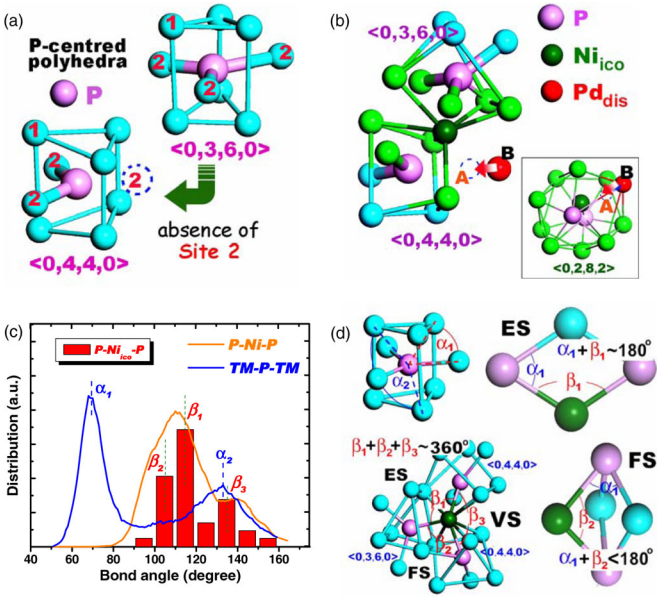


FIG. 4 (color online). (a) The typical atomic configuration of P-centered $\langle 0, 3, 6, 0\rangle$ and $\langle 0, 4, 4, 0\rangle$ clusters as well as the relationship between the two types of clusters. Site 1 denotes the vertices of the trianglar prism, and site 2 denotes the side atoms of the trigonal prism. (b) The hybrid packing between one Ni-centered polyhedron and two P-centered clusters. The inset is the planform view of the Ni-centered polyhedron with the Voronoi index of $\langle 0, 2, 8, 2\rangle$. Sites **A** and **B** represent a special atom site for the switch from $\langle 0, 3, 6, 0\rangle$ to $\langle 0, 4, 4, 0\rangle$ for the P-centered trigonal prism structure and from a symmetric icosahedronlike polyhedron to a low-symmetric atomic cluster. (c) The bond-angle distributions of Ni-vertex and P-vertex angles that reflect the correlation between two neighboring P-centered clusters and the Ni-centered polyhedron. (d) The packing methods between the local ordering clusters. The solute Ni atoms are the dark gray (green) ones.

The universality of the hybrid assembly of the icosahedronlike polyhedra with the $\langle 0, 4, 4, 0\rangle$ and $\langle 0, 3, 6, 0\rangle$ TTPs in $Pd_{40}Ni_{40}P_{20}$ is also verified by the statistic angle distributions. For the P-vertex bond-angle distribution, there are two peaks at ~70° (denoted as $\alpha_1$) and ~130° (denoted as $\alpha_2$) [Fig. 4(c)], corresponding to the P-centered $\langle 0, 4, 4, 0\rangle$ and $\langle 0, 3, 6, 0\rangle$ TTPs, as shown in Fig. 4(d). The distribution of P-Ni-P angles [Fig. 4(c)] with Ni as the center atoms in $\langle 0, 2, 8, 2\rangle$ or $\langle 0, 0, 12, 0\rangle$ icosahedra presents three favorable angles (denoted as $\beta_1$, $\beta_2$, and $\beta_3$) with the following relations: (1) $\beta_1 + \alpha_1 \cong 180°$ and (2) $\beta_1 + \beta_2 + \beta_3 \approx 360°$. As shown in Fig. 4(d), these angles agree with the three possible arrangements of one icosahedronlike polyhedron with two TTPs in the hybrid assembly by face, edge, and vertex sharing. Based on the three hybrid packing schemes, we calculated Ni-Ni, Ni-P, and P-P

bonding lengths, which are also well consistent with their peaks in partial RDFs, as shown in Figs. 1(b) and 1(c).

Interestingly, we found that the atoms at site **B** are always Pd. A separate energy calculation demonstrates that the Pd at site **B** has relatively lower total energy than that at site **A**, but it is opposite for Ni atoms (see Table S1). Therefore, the improved GFA of $Pd_xNi_{80-x}P_{20}$ ($x = 20, 40, 60$), compared to the binary $Ni_{80}P_{20}$, is most likely associated with the possibility that the substitution of Ni by Pd is favorable to the Ni-centered icosahedronlike polyhedra that play a key role in mediating the covalence-dominated TTPs and dense atomic packing of metallic atoms. On the other hand, too much Pd, such as $Pd_{60}Ni_{20}P_{20}$, may give rise to the decrease in the number and packing density of Ni-centered clusters. Since the TTP clusters can fill the space by edge and vertex sharing to form a periodic crystalline structure of $Ni_3P$ [26], the assembly of Ni-centered icosahedra and P-centered $\langle 0, 4, 4, 0\rangle$ distorted TTPs can also prevent the growth of TTPs in a crystalline manner and thus stabilize the disordered structure for better GFA [27].

In summary, we investigated the atomic structure of $Pd_xNi_{80-x}P_{20}$ glasses and found that covalence-dominated TTPs and densely packed icosahedra coexist in the metal-metalloid glasses. The hybrid assemblies simultaneously satisfy the criteria for the charge saturation of the metalloid element and dense atomic packing of metallic elements, leading to the lowest total energy and relatively stable disordered structure. The novel hybrid packing scheme provides atomic insights into the excellent GFA of $Pd_{40}Ni_{40}P_{20}$ and has important implications in understanding the glass formation of metal-metalloid alloys as well as in developing new metallic glasses with improved GFA by atomic-structure–based alloy design.

The EXAFS/XRD experiments are supported by the JASRI/SPring-8 under Proposals No. 2010A1029, No. 2010A1078, and No. 2010B1492. We thank the Center for Computational Materials Science, Institute for Materials Research, Tohoku University, for affording time on the Hitachi SR11000 (model K2) supercomputing system.

*Corresponding author
mwchen@wpi-aimr.tohoku.ac.jp

[1] D. B. Miracle, Nature Mater. **3**, 697 (2004).
[2] A. R. Yavari, Nature (London) **439**, 405 (2006).
[3] Z. P. Lu and C. T. Liu, Phys. Rev. Lett. **91**, 115505 (2003).
[4] M. W. Chen, NPG Asia Materials **3**, 82 (2011).
[5] X. k. Xi, L. l. Li, B. Zhang, W. h. Wang, and Y. Wu, Phys. Rev. Lett. **99**, 095501 (2007).
[6] T. Fujita, K. Konno, W. Zhang, V. Kumar, M. Matsuura, A. Inoue, T. Sakurai, and M. W. Chen, Phys. Rev. Lett. **103**, 075502 (2009).
[7] Y. Q. Cheng, E. Ma, and H. W. Sheng, Phys. Rev. Lett. **102**, 245501 (2009).
[8] H. W. Sheng, W. K. Luo, F. M. Alamgir, J. M. Bai, and E. Ma, Nature (London) **439**, 419 (2006).
[9] A. Hirata, P. Guan, T. Fujita, Y. Hirotsu, A. Inoue, A. R. Yavari, T. Sakurai, and M. Chen, Nature Mater. **10**, 28 (2011).
[10] T. Egami, W. Dmowski, Y. He, and R. B. Schwarz, Metall. Mater. Trans. A **29**, 1805 (1998).
[11] T. Takeuchi, D. Fukamaki, H. Miyazaki, K. Soda, M. Hasegawa, H. Sato, U. Mizutani, T. Ito, and S. Kimura, Mater. Trans., JIM **48**, 1292 (2007).
[12] N. Nishiyama and A. Inoue, Acta Mater. **47**, 1487 (1999).
[13] A. Hirata, Y. Hirotsu, and E. Matsubara, Mater. Trans., JIM **46**, 2781 (2005).
[14] P. H. Gaskell, Nature (London) **276**, 484 (1978).
[15] T. Egami and Y. Waseda, J. Non-Cryst. Solids **64**, 113 (1984).
[16] A. J. Drehman, A. L. Greer, and D. Turnbull, Appl. Phys. Lett. **41**, 716 (1982).
[17] G. Kresse and J. Furthmuller, Phys. Rev. B **54**, 11 169 (1996).
[18] M. P. Allen and D. J. Tidesley, *Computer Simulation of Liquids* (Oxford University Press, New York, 1987).
[19] P. E. Blöchl, Phys. Rev. B **50**, 17 953 (1994).
[20] Y. Wang and J. P. Perdew, Phys. Rev. B **44**, 13 298 (1991).
[21] See Supplemental Material at http://link.aps.org/supplemental/10.1103/PhysRevLett.108.175501 for the details of simulation, experiment, and structure analysis of $Pd_xNi_{80-x}P_{20}$ ($x = 0, 20, 40, 60$) glasses, as well as the hybrid packing method.
[22] Y. He, R. B. Schwarz, and J. I. Archuleta, Appl. Phys. Lett. **69**, 1861 (1996).
[23] J. L. Finney, Nature (London) **266**, 309 (1977).
[24] The frequencies are normalized by the atomic numbers of P. Since the four alloys have the same P atoms, the normalized frequencies reflect the true number of Ni-centered polyhedra and their intrinsic correlation with P-centered clusters.
[25] Since we did not relax the atomic configuration with Pd at site **A**, we can only get the primary energy barrier. We used several different atomic configurations for the energy barrier calculation, and the average value is about 0.08 eV/atom.
[26] S. Rundqvist, Arkiv. Kemi **20**, 67 (1962).
[27] H. Shintani and H. Tanaka, Nature Phys. **2**, 200 (2006).